IEEE Photonics Journal
An IEEE Photonics Society Publication

Open Access

LED and CMOS Image Sensor Based Optical Wireless Communication System for Automotive Applications

Volume 5, Number 5, October 2013

Isamu Takai, Member, IEEE
Shinya Ito
Keita Yasutomi, Member, IEEE
Keiichiro Kagawa, Member, IEEE
Michinori Andoh
Shoji Kawahito, Fellow, IEEE

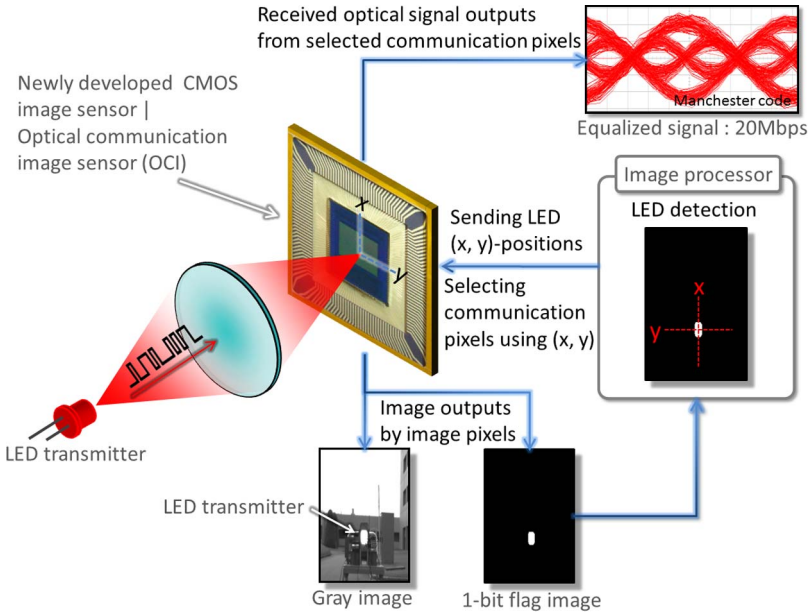

DOI: 10.1109/JPHOT.2013.2277881
1943-0655

IEEE photonics SOCIETY

IEEE

LED and CMOS Image Sensor Based Optical Wireless Communication System for Automotive Applications

Isamu Takai,[1,2] *Member, IEEE*, Shinya Ito,[2] Keita Yasutomi,[2] *Member, IEEE*, Keiichiro Kagawa,[2] *Member, IEEE*, Michinori Andoh,[1] and Shoji Kawahito,[2] *Fellow, IEEE*

[1]Applied Optics Laboratory, Toyota Central R&D Laboratories, Inc., Nagakute 480-1192, Japan
[2]Research Institute of Electronics, Shizuoka University, Hamamatsu 432-8011, Japan

DOI: 10.1109/JPHOT.2013.2277881

Manuscript received July 15, 2013; accepted August 4, 2013. Date of publication August 8, 2013; date of current version September 4, 2013. This work was supported in part by the Knowledge Cluster Initiative of the Ministry of Education, Culture, Sports, Science and Technology (MEXT). Corresponding author: I. Takai (e-mail: takai@mosk.tytlabs.co.jp).

Abstract: An optical wireless communication (OWC) system based on a light-emitting-diode (LED) transmitter and a camera receiver has been developed for use in the automotive area. The automotive OWC system will require Mb/s-class data rates and the ability to quickly detect LEDs from an image. The key to achieving this is improvements to the capabilities of the image sensor mounted on the camera receiver. In this paper, we report on a novel OWC system equipped with an optical communication image sensor (OCI), which is newly developed using CMOS technology. To obtain higher transmission rates, the OCI employs a specialized "communication pixel (CPx)" capable of responding promptly to optical intensity variations. Furthermore, a new quick LED detection technique, based on a 1-bit flag image which only reacts to high-intensity objects, is formulated. The communication pixels, ordinary image pixels, and associated circuits (including 1-bit flag image output circuits) are then integrated into the OCI. This paper describes the design, fabrication, and capabilities of the OCI, as well as the development of the LED and image sensor based OWC system, which boasts a 20-Mb/s/pixel data rate without LED detection and a 15-Mb/s/pixel data rate with a 16.6-ms real-time LED detection.

Index Terms: Optical wireless communication (OWC), visible light communication (VLC), light-emitting diode (LED), complementary metal–oxide–semiconductor (CMOS) image sensor, image sensor based OWC, automotive communication system.

1. Introduction

Recently, optical wireless communication (OWC) systems based on light emitting diode (LED) transmitters have attracted significant attention as next-generation communication systems [1]–[4]. Especially, the OWC using visible light LEDs are referred to as visible light communication (VLC) [5]–[10]. Such systems are expected to be particularly useful in automotive applications aimed at enhancing driving safety and comfort [11]–[14]. LEDs are highly suitable for use as OWC transmitters because they can modulate at very high speeds in comparison to traditional light sources such as incandescent light bulbs and fluorescent lamps, and because LEDs have already been used for various light sources in automotive fields, including headlights, taillights, brake lights, and traffic lights. This background provides a foundation for the practical achievement of automotive OWC systems.

As receivers, cameras are considered up-and-coming candidates [15]–[19]. Analogous with LEDs, cameras have also been integrated into and widely used in a number of vehicle applications. Accordingly, it is felt that if an already existing vehicle camera could be merged with the OWC system, it would result in a relatively low-cost communication system because many of the camera system components could be shared. Moreover, if the camera is used, the OWC system would possess characteristics not found in other wireless communication technologies owing to structures of an image sensor mounted on the camera receiver. This image sensor based OWC (IS-OWC) would enable noninterference communication, facilitate the identifications of exact spatial positions of transmitters from captured images, and provide other benefits as well [19]. Furthermore, the fusion of results obtained via image processing and received communication data could be expected to prompt the emergence of new applications in the future.

As potential drawbacks of this system, since the optical channels are line-of-sight (LOS), its communication links will be blocked by objects that prevent light penetration, such as walls, buildings, thick fog, and thick gas.

A few approaches using image sensors for a high-speed optical signal reception have already been reported [20]–[23]. A frame rate of commonly used image sensors is approximately 30 frames per second (fps). If its frame rate is assumed to be 30 fps, the data rate per pixel must be limited to 15 bit per second (bps) or less to satisfy the Nyquist frequency requirement. Accordingly, in these reported approaches, in order to achieve higher data rates, or receive high-speed optical signals, high speed cameras or newly developed image sensors have been used in the receiver systems. However, the systems using the new image sensor have been developed for ID beacon signal reception, not for large data reception. Therefore, their data rates are limited to a range from several kbps to tens of kbps per pixel. Also, data rates per pixel of the high speed camera systems is limited to tens of kbps per pixel or less [15] because of response bounds of a pixel, working speed limits of circuits in an image sensor, and/or performance constraints of external circuits such as memory speeds, its sizes, and processing speeds of various devices. The actual required data rates depend on the adopted applications. However, in order to send and receive an enormous volume of vehicle internal data and traffic information data promptly, Mbps-class performance would be needed. Furthermore, if the transmission of larger multimedia data (such as image and video data) is required, even higher data rates would be needed. Thus, when working to apply IS-OWC to automotive systems, one of the keys is that the data rate is improved to Mbps level. Of course, if the data rate is enhanced, the application range of this system would be extended as well.

In addition, when the IS-OWC system is used in automotive systems, real-time LED detection is a very important function because the spatial positions (x- and y-coordinates) of LEDs on images will change with each frame because of the constant motion of the LED transmitter and camera receiver at high speeds. Such systems must also contend with the vibration, pitching, and rolling motions of each vehicle. Thus, if LED positions cannot be quickly and accurately detected from the image, long communication blackouts could result. Therefore, when the IS-OWC system is used for automotive applications, quick and accurate LED detection capabilities, along with low calculation costs, are essential requirements.

This paper introduces a novel IS-OWC system based on an LED transmitter and camera receiver along with a newly developed image sensor, which is intended for automotive applications, including vehicle-to-vehicle and vehicle-to-infrastructure communication systems. The target data rate is 10 Mbps per pixel or more for simultaneously sending color video data and vehicle internal data, such as vehicle speed, braking status, etc. Additionally, for communicating while vehicles are moving, the target LED detection rate is 16.6 ms, which is considered to be a real-time detection.

Toward this goal, we develop an optical communication image sensor (OCI) using complementary metal-oxide-semiconductor (CMOS) technology that can integrate multiple functions. For achieving the required data rate, a specialized pixel for communication, "communication pixel (CPx)", is designed using pinned photodiode (PD) technology [24], which provides substantially improved response to light intensity variations when compared to conventional imaging pixels. In addition, for real-time LED detection, a new detection technique that uses "1-bit flag image" is

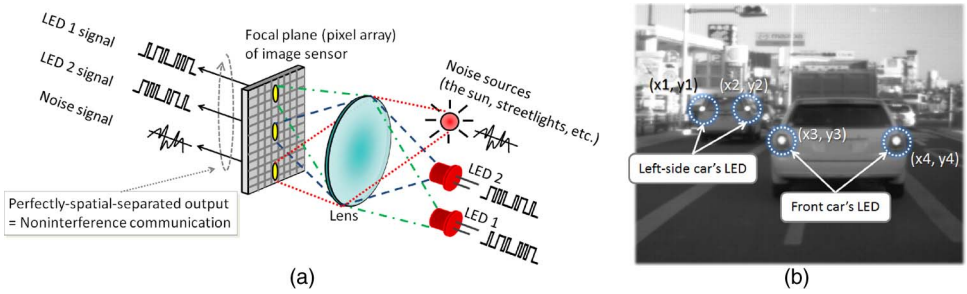

Fig. 1. Characteristics of the IS-OWC system. (a) Noninterference communication. (b) Identifications of sources.

proposed, and implementing this flag image obtainment function allows the quick and highly accurate LED detection.

This paper describes the design, implementation, and evaluation results of the OCI, and presents development results and empirical performances of the IS-OWC system using the OCI. Additionally, this paper shows the results of the world's first 20 Mbps per pixel transmission combined with the 16.6 ms real-time LED detection.

2. Characteristics of IS-OWC Technology

Owing to the structure of an image sensor, the IS-OWC system has several beneficial characteristics [5] that are not found in other wireless communication systems such as systems using radio waves or single-element PDs [12], [13].

One of these is noninterference communication [19] as shown in Fig. 1(a). When an image sensor is used as a receiver, light sources are almost perfectly separated on a focal plane (a pixel array) because there are a massive number of pixels, and optical signals are separately output from each pixel. This prevents signals from becoming mixed, thus allowing communication, even if many LED transmitters and superfluous lights (noise sources) such as sunlight and streetlights are present.

This capability provides high S/N communication, requires no complicated protocol use for simultaneous communication with multi-LEDs, and provides the ability to accept different protocol signals by each LED. This feature is very helpful for automotive applications that must be performed under real road environments, where numerous superfluous light sources exist and where simultaneous communication with multiple vehicles and traffic signals is necessary.

Additionally, as shown in Fig. 1(b), when the IS-OWC system receives optical signals, the spatial position, exact (x, y)-coordinates, of the LEDs can also be obtained from the image [15]. As a result, the receiver-side system can easily and clearly identify sources of received data such as a car traveling on the left or a car directly ahead without complex processing or GPS positioning data. Furthermore, since users can freely select communication partners from an image, there is no need for the complex signal processing required to filter out superfluous information because the LEDs that are not needed by receivers can be disregarded entirely.

As with the other system characteristics, the optical signal power received by the IS-OWC is stable against changing communication distances. More specifically, the incident light power per pixel remains unchanged, despite communication distance variations, as long as the imaged LED size on the focal plane of the image sensor is larger than the pixel size [25]. Fig. 2 shows a calculation result of the received signal power per pixel as a function of the communication distance. As can be seen in the figure, the result is stable up to 80 m under the conditions of a pixel size of 7.5×7.5 μm^2, an LED array size of 10×10 cm^2, and a lens focal length of 6 mm. If the distance exceeds 80 m, the received signal power is reduced because the size of the imaged LED is smaller than the pixel size. Of course, the optical signal can be received in outside of the stable range if an S/N ratio requirement is satisfied. This feature is helpful for achieving stable quality communication.

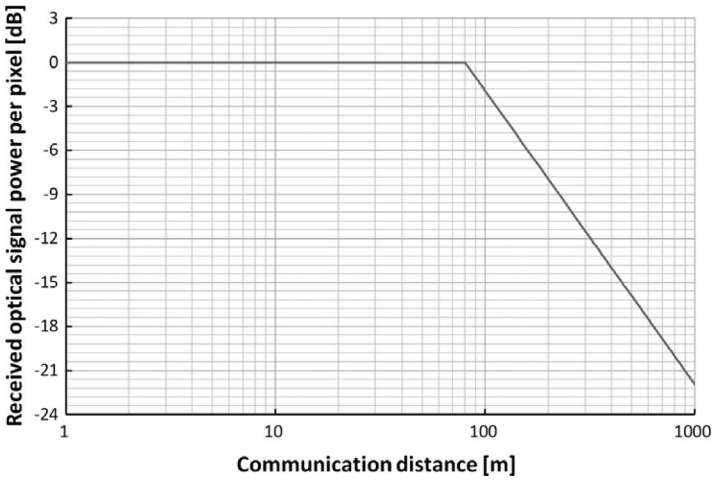

Fig. 2. Received optical signal power per pixel vs. communication distance.

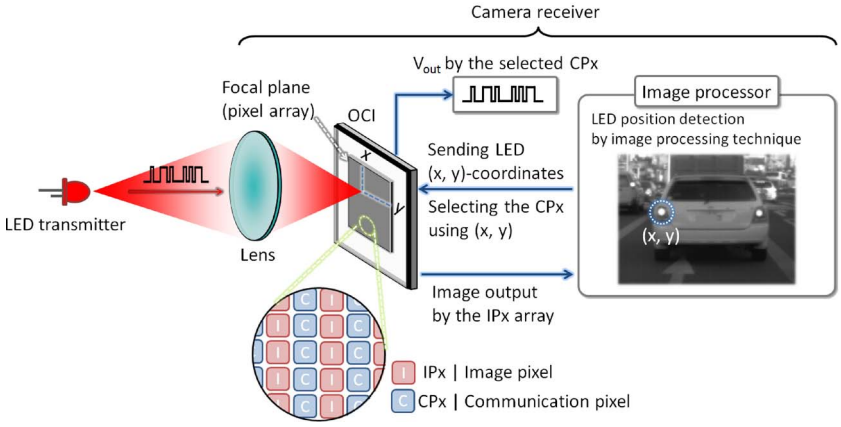

Fig. 3. Basic operations of IS-OWC system.

If a longer focal length lens is used, the maximum stable power distance is lengthened by a zoom effect. However, on the other side of the coin, an angle of view is narrowed. In accordance with application requirements, a proper lens selection is important.

3. The OCI Chip Design for IS-OWC System

3.1. Basic Operations of IS-OWC System

Fig. 3 shows the basic operations of the IS-OWC system proposed in this paper. The newly developed CMOS image sensor, the OCI, is employed to this system. Optical signals transmitted from a LED transmitter strike the focal plane (pixel array) of the OCI through the lens of a camera receiver, and are received by pixels that are hit by incoming optical signals. The OCI pixel array consists of an image pixel (IPx) array for imaging and the CPx array for communication. This system is initiated by the output of image signals for LED detection. The image signals obtained by the IPx array are delivered to an external image processor and the LED positions, (x, y)-coordinates, are detected by image processing techniques. The obtained coordinate data is sent back to the OCI. Next, the optical signals are received by the CPx corresponding to the (x, y)-coordinate, and is then output from the OCI through its readout circuits. This operation, which is

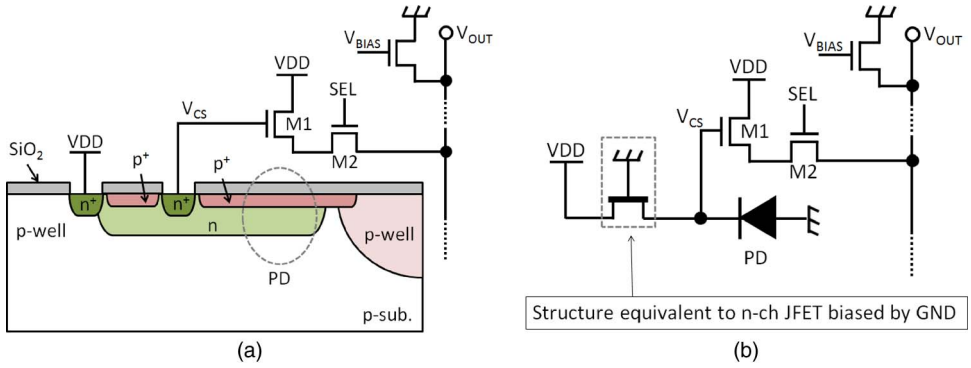

Fig. 4. Overview of CPx structure. (a) CPx cross-section. (b) CPx schematic.

repeated constantly in real-time, permits this system to receive the optical signals while the LED is being detected.

The key challenges faced by the OCI are twofold: the development of a CPx capable of high-speed optical signal reception for 10 Mbps or more transmission, and the implementation of a 1-bit flag image output function for 16.6 ms real-time LED detection.

3.2. Structures and Operations of the CPx

Fig. 4 shows a simplified cross-section and schematic of the CPx developed for high-speed optical signal reception. The CPx consists of two transistors, a PD, and a component equivalent to an n-channel junction gate field-effect transistor (n-ch JFET) biased by GND. A charge-sensing node (voltage: V_{CS}) is connected to PD and that component coupled to a power supply voltage (V_{DD}). Additionally, the sensing node is connected to the gate of transistor M1, which is used for a source follower readout amplifier. The M2 transistor is used for CPx selection.

This simple structure makes a significant contribution to the high sensitivity of the CPx because the PD area size for photo detection can be expanded due to the decreasing number of transistors. However, increasing the capacitance according to expansion of PD area size typically results in degraded response performance. Therefore, in order to balance the competing goals of high speed response and high sensitivity, a depleted PD with a floating diffusion (FD) and charge overflow drain is used as the PD of the CPx. Use of a depleted PD implemented with pinned PD technology is helpful for enhancing the time response while achieving high sensitivity because the capacitance in the depletion region is significantly reduced when the fringing field is created. Additionally, due to the structure of the lateral charge overflow drain, the V_{CS} response to a light intensity, or photo-current, is logarithmic [24]. This feature prevents the output signal from becoming saturated by strong intensity light, thus making it wide working light power ranges.

Fig. 5 shows the operation of CPx with a potential profile and V_{CS} response. When the signal condition is ON, if an optical signal enters the PD area, electric charges corresponding to the light intensity are generated by photoelectric conversion and are immediately transferred to the charge-sensing node (FD part). After transferring to the FD, these charges are drained to V_{DD}. The V_{CS} level decreases rapidly in a logarithmic response to the increasing number of charges. Since there is no transistor to handle charge transfers in the CPx, the generated charges are continuously discarded to the drain. When the signal condition is OFF, the residual charge stored in the PD and FD is drained to V_{DD}, after which the V_{CS} increases in a curve that is logarithmic to the charge decrease. Since the OFF response is dominated by diffusion current, it is slower than the ON response. Therefore, the response performance of the CPx is determined by OFF response, or rise time. To summarize, the response characteristics of the CPx is an asymmetric logarithm.

In this type of pixel, the capacitance has a direct effect on response performance. Accordingly, in order to reduce the charge sensing node capacitance, the FD size has been reduced to the maximum extent possible. Additionally, in comparison to the response of a previous design [26] that

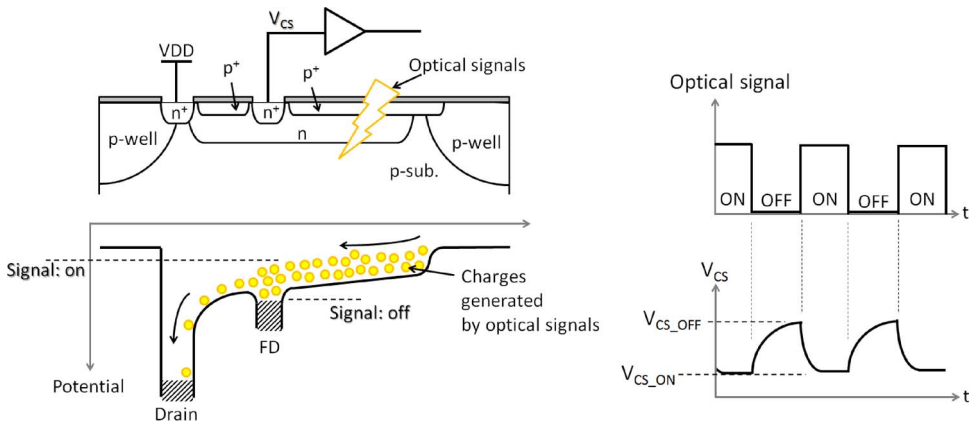

Fig. 5. CPx operations.

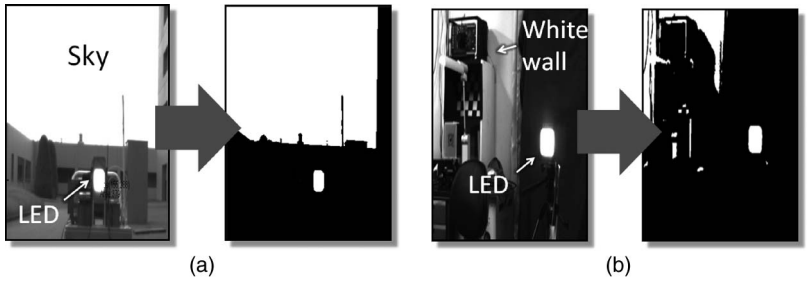

Fig. 6. LED detection using gray images. (a) Example 1: outdoor. (b) Example 2: indoor.

used the sub-threshold operation of a MOSFET, this structure is faster because it has no influence of the gate-to-source capacitance of transfer transistors and because the larger PD improves sensitivity.

3.3. 1-Bit Flag Image Output Function

As shown in Fig. 6, a common LED detection method utilizes a simple binarized image generated from a gray image. However, in actual indoor and outdoor images, numerous superfluous objects with high light intensity values, such as sky regions and white walls, tend to be present. As a result, it is very difficult to detect LED regions precisely and rapidly from such images at low calculation costs.

In response to this issue, we propose a new detection method using a 1-bit flag image. In gray images, the LED, sky, and wall regions are all saturated, which means that the light intensity of such areas appears to be identical. However, in actuality, the light intensity level of an LED in direct view is significantly larger than that of other objects. Therefore, focusing on this fact, the IPx array outputs a new image signal whose charge accumulation time is reduced to 1/480 that of gray image. A comparator circuit then binarizes this very short exposure time image signal and outputs it as a "1-bit flag image". In this flag image, due to the very short time exposure, only high-intensity light objects such as LEDs, the Sun, and streetlights will react and register as "1"s, whereas low-intensity objects will disappear from the image. Using this 1-bit flag image for LED detection significantly reduces calculation costs and achieves real-time detection because almost all superfluous objects are eliminated. Of course, detection accuracy is significantly improved in contrast to methods using usual gray images.

In this paper, the OCI employs output functions of not only 1-bit flag image for the LED detection, but also gray image for future use in image processing based automotive safety applications such as lane departure warnings, collision warnings, and pedestrian detection.

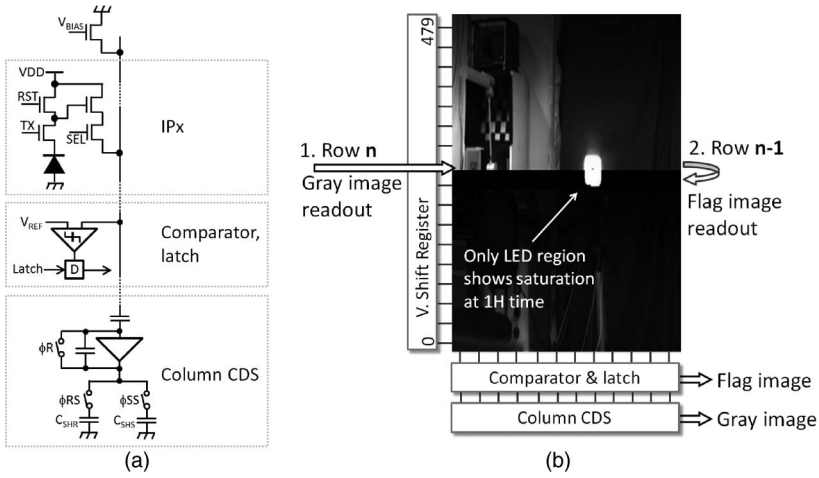

Fig. 7. Outline of image readout circuits. (a) Column readout circuits. (b) Readout circuit operation.

Fig. 7(a) shows the column readout circuits for 1-bit flag image and gray image output. As can be seen in the figure, the IPx consists of a standard four-transistor active pixel structure (4-Tr APS) with a pinned PD [27], [28]. Almost all of the circuits and operations are identical to those of the conventional 4-Tr APS [29]. To permit LED detection, it is only necessary to add a comparator and latch circuits to each column, which is then connected to an IPx output line with a correlated double sampling (CDS) circuit.

Fig. 7(b) shows the column readout circuit operations that perform two functions: the low-noise gray image signal readout using CDS operation and the 1-bit flag image readout using comparator circuits with short accumulation time. As can be seen in the figure, IPx outputs are connected to the bottom column readout circuits. The process begins when nth gray image signals are output through the CDS circuit. After the nth CDS operation, the minus 1 (n-1 th) neighbor row is selected by a vertical shift register, and the signal of that row is output through the comparator circuit as the 1-bit flag image signal. Despite an accumulation time of just 1H time, the LED location on the IPx array is nearly saturated because of the overwhelming intensity of LED light in comparison to that of other objects. After this operation is repeated from the 0th to 479th row, the gray image and flag image are completed on external circuits. In this system, both images are obtained simultaneously at 60 fps, and LED detection using this flag image is executed on the external circuit in a period of approximately 16.6 (1/60) ms. Thus the 1H time is approximately 35 μs (1/60 fps/480 rows).

3.4. The Block Diagram of the OCI Chip

Fig. 8 shows a block diagram of the OCI chip. As previously explained, it has two functions, one of which is for taking images and the other of which is for receiving optical signals. In the pixel array, the IPx array and the newly designed CPx array are set to odd and even columns in alternate shifts.

As for peripheral circuits, the image signal readout circuits are set at the bottom of the pixel array. These consist primarily of the Vertical (V.) and Horizontal (H.) shift registers, the column comparator with latch, the column CDS circuits, and the readout amplifiers. The communication signal readout circuits are set at the top of the pixel array. These include the X- and Y- address generator, the nine-channel (9-ch) column selector, and the 9-ch readout amplifiers.

We will now provide a complete overview of the OCI chip operation, which is initiated by 1-bit flag image output and LED detection. First, LED regions are detected within a 16.6 ms period via an image processing technique on an external circuit such as a digital signal processing (DSP) unit, and the central (x, y)-coordinate data of the detected LED area is delivered to the X- and Y- address generator of the OCI, after which the CPx selected by the address generators is activated and receives the optical signals. In this OCI chip, as shown in Fig. 9, a (x′, y)-CPx neighboring the

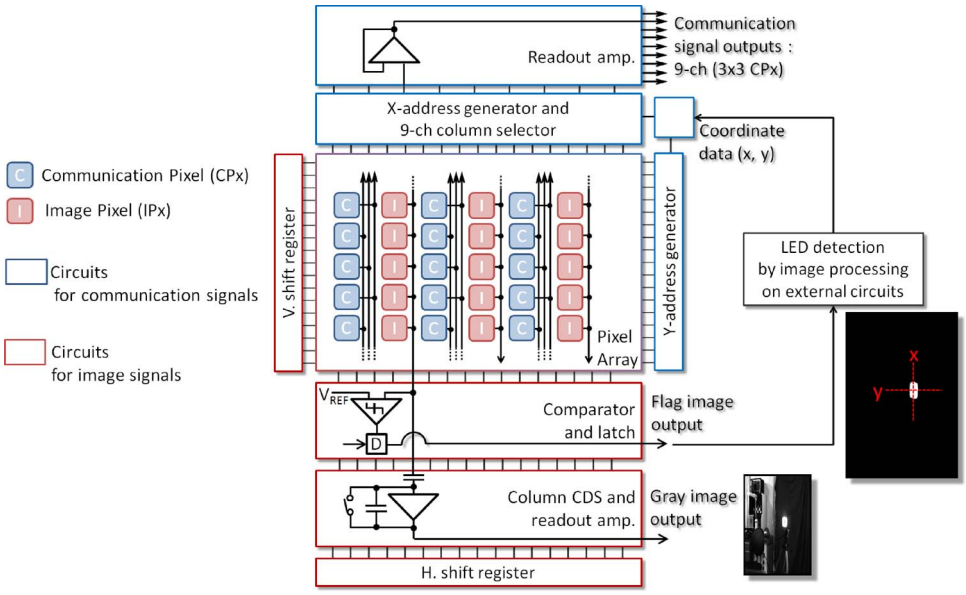

Fig. 8. Block diagram of the OCI chip.

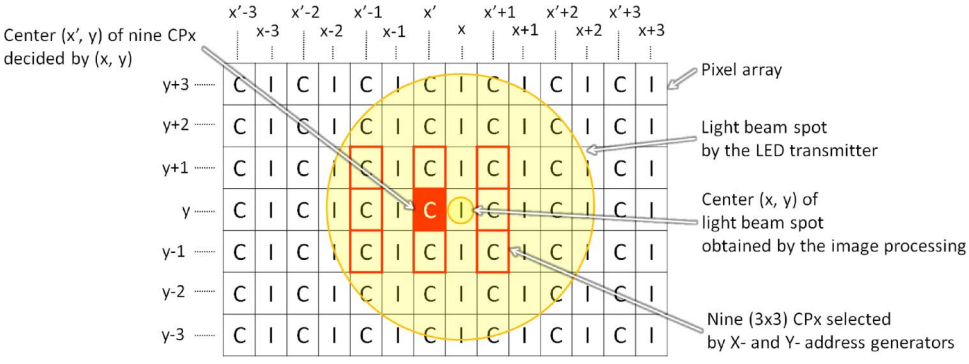

Fig. 9. Selecting the nine CPx.

obtained (x, y)-IPx is selected by address generators. Additionally, nine (3×3) CPxs with a central focus on (x′, y)-CPx are selected simultaneously. These nine selected CPxs provide a margin area in the event the LED (light beam spot) moves slightly from the obtained (x, y)-position within 16.6 ms, which allows communication to be maintained. Finally, the nine optical signals received by the selected nine CPxs are output through the 9-ch column selectors and 9-ch readout amplifiers. This entire operation is repeated every 16.6 ms and allows the OCI to receive a high-speed optical signal while continuously detecting the LED in real-time.

3.5. Chip Implementation

The OCI chip is designed and implemented using a typical 0.18 μm CMOS image sensor (CIS) technology with pinned PD. Fig. 10 shows a photograph of the fabricated 7.5 mm $\times$ 8.0 mm OCI chip. A 642 $\times$ 480 pixel array consists of a 321 $\times$ 480 IPx array and a 321 $\times$ 480 CPx array. Pixel sizes of the IPx and CPx are 7.5 μm $\times$ 7.5 μm. Since color filters are not set on the CPx array, the CPx can receives optical signals whose wavelengths range from visible light to near-infrared light (about 400 nm to 900 nm). The parameters of the OCI chip are summarized in Table 1.

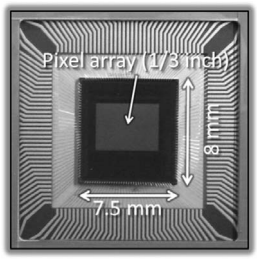

Fig. 10. Photograph of the fabricated OCI chip.

TABLE 1

Specifications of the OCI chip

Technology	0.18 µm 1P4M CIS
Chip size	7.5(H) mm × 8.0(V) mm
Pixel size	7.5(H) µm × 7.5(V) µm
Pixel array size	642(H) × 480(V) - IPx: 321(H) × 480(V) - CPx: 321(H) × 480(V) 4.8 mm × 3.6 mm (1/3 inch)
Power supply	1.8V to digital circuits 3.3 V to analog circuits

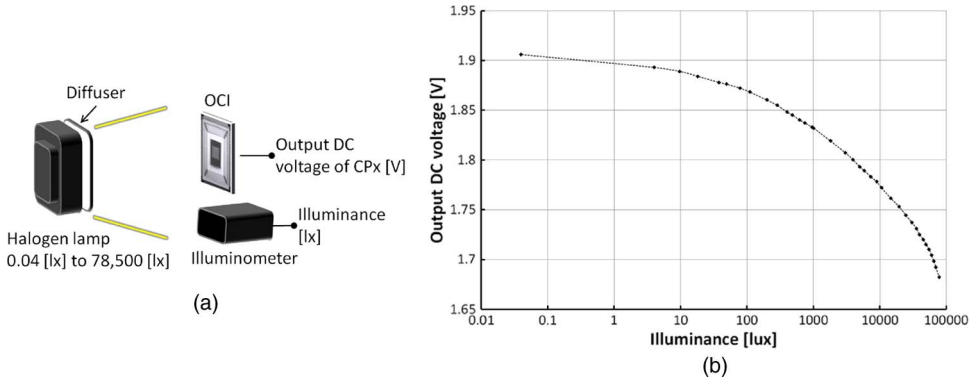

Fig. 11. Measurement of DC response characteristics. (a) Measurement setup. (b) Measurement result.

4. Evaluations of CPx

4.1. DC Response

Fig. 11(a) shows the setup used to measure the DC light response characteristics of a single CPx. The light intensity is intergraded by using a halogen lamp set facing the OCI radiating from 0.04 lx to 78,500 lx, after which the output voltage of the CPx through the read amplifier is measured. This intensity range is meant to simulate outdoor light conditions. No lens is used during this measurement and a 1 m distance is set between the halogen lamp and the OCI.

Fig. 11(b) shows the measurement results of the DC light response of a CPx as a function of illuminance. As can be seen in the figure, when the light conditions change from 0.04 lx (nighttime) to 78,500 lx (daytime), the output voltage swings from 1.90 V to 1.68 V, thus ΔV is 220 mV. Due to structure of the lateral charge overflow drain, response to light intensity is logarithmic, and it is

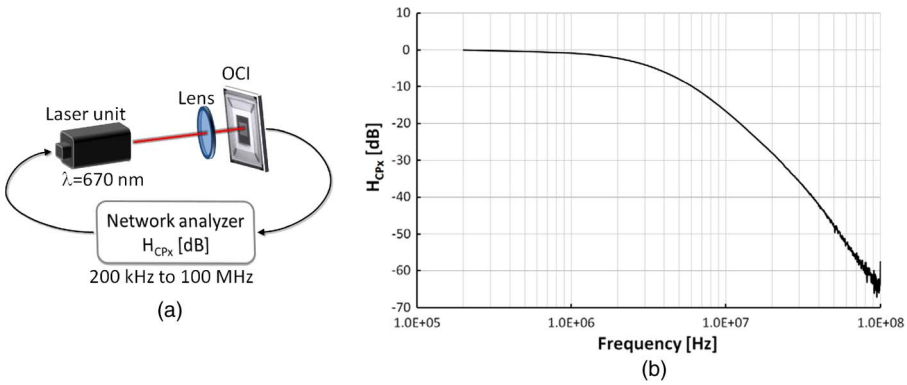

Fig. 12. Measurement of frequency response characteristics. (a) Measurement setup. (b) Measurement result.

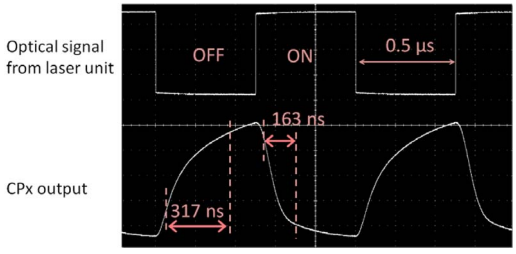

Fig. 13. Measurement result of transient response characteristics.

confirmed that the CPx does not become saturated even under the very strong light conditions. More specifically, the CPx can receive optical signals under almost all outdoor light conditions without becoming saturated, which has significant implications for its utility in automotive applications. Furthermore, this result shows that the offset level of the CPx output constantly changes due to the background light level, thus DC-free coding methods for data transmission should be used.

4.2. Frequency Response

Fig. 12(a) shows the setup for measuring the frequency response characteristics of the single CPx. In this experiment, the light source is a laser of $\lambda = 670$ nm and BW = 100 kHz to 2.5 GHz. An $f = 4.2$ mm and $F_N = 1.6$ lens is used. The frequency response, H_{CPx} as a transfer function of each frequency, is measured by a network analyzer that drives the laser unit via 200 kHz to 100 MHz signals. The number of measuring frequency points is 1601 with 10 times averaging.

Fig. 12(b) shows the measurement results of the frequency response characteristics. From this result, it is found that H_{CPx} continuously declines as the frequency increased, for example -20 dB at 11.5 MHz and -40 dB at 36 MHz compared to a base of 200 kHz. There is no flat region in a band used for 10 Mbps class transmission, such as around 10 MHz. It is due to the logarithmic response characteristics of the CPx. Because of this, when optical signals of 10 Mbps class are received by the CPx, the CPx output signal will be distorted. In this study, an equalizer circuit is employed to correct this distorted signal, and this H_{CPx} characteristic is utilized for equalizer designs.

4.3. Transient Response

Fig. 13 capturing an oscilloscope display monitor shows the measurement result of a single CPx transient response receiving a 1 MHz and approximately 0.5 mW laser pulse optical signals. The top signal of this figure is the optical signal of the laser unit, while the bottom is the CPx output.

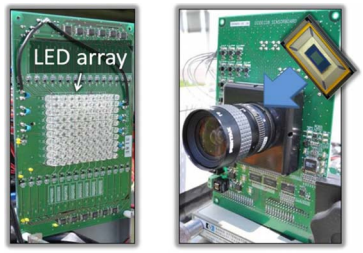

Fig. 14. Sample IS-OWC system. (a) LED transmitter. (b) Camera receiver.

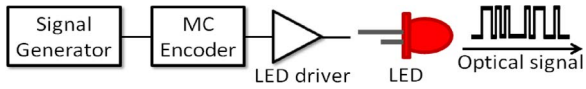

Fig. 15. LED transmitter System block diagram.

TABLE 2

Specifications of LED transmitter

Modulation method	On-Off-Keying (OOK)	
Encoding method	Manchester Coding (MC)	
Data rate	10 M, 15 M, 20 Mbps	
LED array size	5.5 cm × 5.5 cm	
Peak emission wavelength	870 nm (near-infrared)	
Optical output power	up to 2 W	
Half intensity angle	40 deg.	
Measured cut-off frequency	55 MHz (Fig. 16 (a))	
Measured rise time	4.2 ns	(Fig. 16 (b))
Measured fall time	7.1 ns	

These results show that rise time (10% to 90%) and fall time (90% to 10%) of the CPx output are different, asymmetric curve shapes, and that the rise time is longer than that of the fall, which is consistent with the explanations described in the previous section. Under these experimental conditions, the difference is approximately a factor of 2. These measurement results show that the rise time determines the CPx response performance.

5. Development of IS-OWC System and Experiments

5.1. IS-OWC System

Fig. 14 shows an example IS-OWC system consisting of an LED transmitter and a camera receiver containing the OCI.

Fig. 15 and Table 2 show the system block diagram and specifications of the LED transmitter, respectively. Transmission signals are encoded in Manchester Code (MC), which is a DC-free coding method, and coded signals are transmitted to the camera receiver by optical signals through a free space. This transmitter can select three data rates, 10 (9.765625) Mbps, 15 (15.625) Mbps, and 20 (19.53125) Mbps. The transmitter has 100 LEDs in a 5.5 cm $\times$ 5.5 cm area. LEDs emit up to 2 W of 870 nm near-infrared light. The cut-off frequency is 55 MHz from the frequency response measurement results shown in Fig. 16(a). The measured response performance are a rise time of

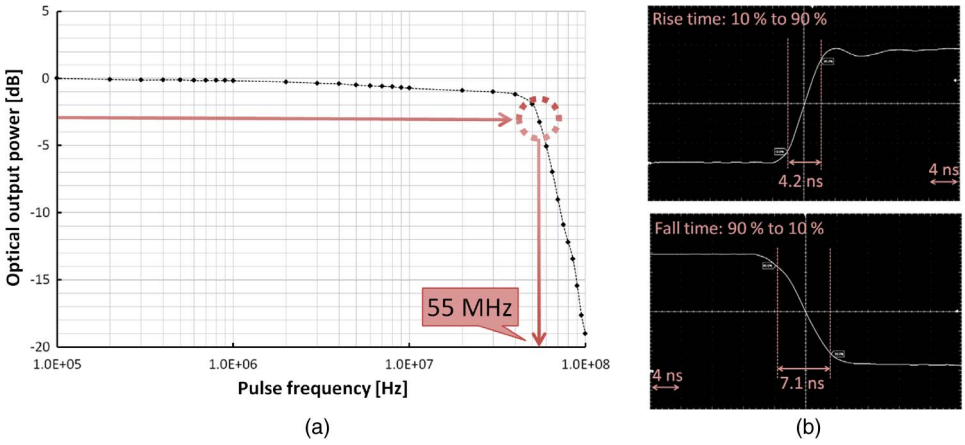

Fig. 16. Measurement results of LED transmitter performances. (a) Frequency response. (b) Transient response.

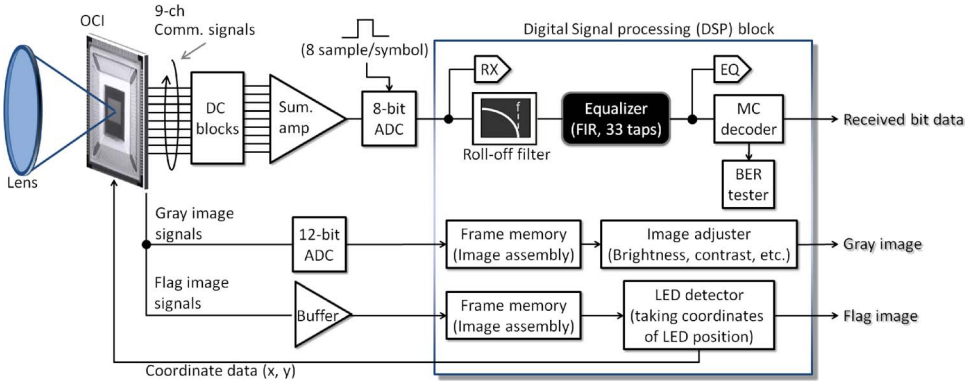

Fig. 17. System block diagram of the camera receiver.

4.2 ns and a fall time of 7.1 ns as shown in Fig. 16(b). Therefore, this LED transmitter has sufficient capability to transmit an optical signal at a data rate exceeding 10 Mbps. In this paper, near-infrared LEDs are used, however, visible light LEDs can also be used for this system.

Fig. 17 shows the system block diagram of the camera receiver. This camera receiver can receive a high-speed optical signal and detect LEDs in real-time.

We will now describe the processing flow of received and output communication signals. First, the 9-ch signals output from the OCI are summed by a summing amplifier with blocking DC components. The summed signal is then digitalized by an 8-bit analog-to-digital converter (ADC), after which it is delivered to a DSP block. The ADC sampling rate is set to 8 times of the data rate (8 sample/symbol). On the DSP block, the input signal is subjected to digital filter processing using a roll-off filter and equalizer to correct for distorted signals in the frequency domain. The equalizer consists of a transversal (FIR: finite impulse response) filter that has 33 taps. The tap coefficients are once calculated by the recursive least square (RLS) algorithm, after which they are fixed. Finally, the equalized signal is decoded and output as the received bit data. A bit error rate (BER) can be also measured using a BER tester.

The gray and flag image signals are output from individual pins of the OCI at a clock speed of approximately 10 MHz. Each signal is then stored to frame memory, and the gray and flag images are assembled. After gray image assembly is complete, image processing is executed to adjust, for example, brightness, contrast, and gamma. The flag image is used to ascertain the coordinate of LED positions on the LED detector block using a classical connected-component labeling algorithm

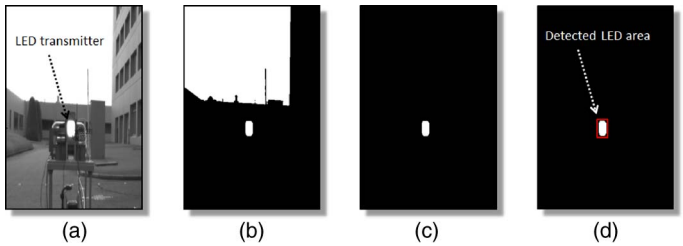

Fig. 18. Experimental results of LED detection under outdoor conditions. (a) Gray image. (b) Binarized gray image. (c) Flag image. (d) Detection result.

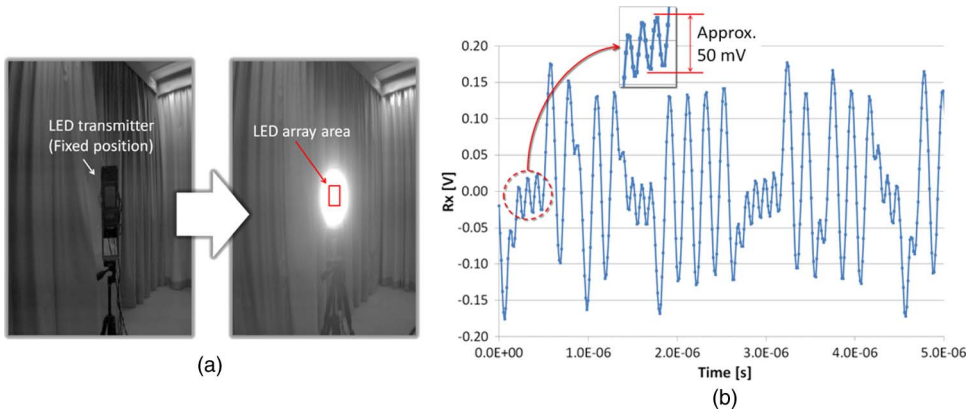

Fig. 19. Experiment of 10 Mbps MC signal reception. (a) Measurement setup. (b) Reception result.

[30]. Finally, the obtained (x, y)-coordinate data is delivered to the OCI in a period of 16.6 ms. In this paper, the gray image is only used for display purposes. However, in the future, it may be used for various common automotive safety applications.

5.2. Experimental Results of LED Detection

Fig. 18 shows the results of LED detection experiments conducted under outdoor light conditions. Fig. 18(a) is a gray image, Fig. 18(b) is a simple-binarized gray image, Fig. 18(c) is an output result of the 1-bit flag image, and Fig. 18(d) is an LED detection result.

Prior to this research, gray images binarized via simple algorithms were used for LED detection, as shown in Fig. 18(b). However, it is extremely difficult to accurately extract LED regions when the image contains superfluous high-intensity objects such as the sky. In contrast, superfluous objects, such as sky regions, can be eliminated perfectly from a 1-bit flag image, as shown in Fig. 18(c), which allows the LED region to be easily and quickly detected via a simple image processing method at low calculation costs, as shown in Fig. 18(d). Furthermore, since the misdetection ratio will also decrease, due to the use of this flag image, quick and accurate LED detection can be achieved even in actual road environments.

5.3. 10 Mbps Signal Reception Experiment

Fig. 19(a) shows the LED transmitter setup conditions for a 10 Mbps signal reception experiment. Here, the LED transmitter position is fixed and the LED detection function is stopped after the LED area is detected one time. The distance between the LED transmitter and the camera receiver is set at 1 m, and a lighting condition is 350 lx. An $f = 4.2$ mm, $F_N = 1.6$ lens is used. MC random data (PN9) is transmitted at 10 Mbps. The received (RX) and equalized (EQ) signals are monitored via their respective pins, as shown in Fig. 17.

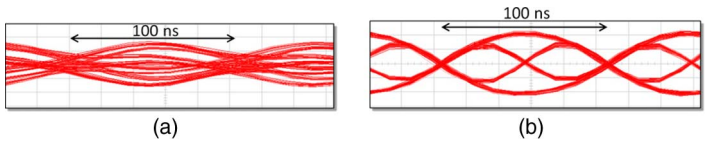

Fig. 20. Eye diagrams of RX and EQ output at 10 Mbps MC signal reception. (a) RX signal. (b) EQ signal.

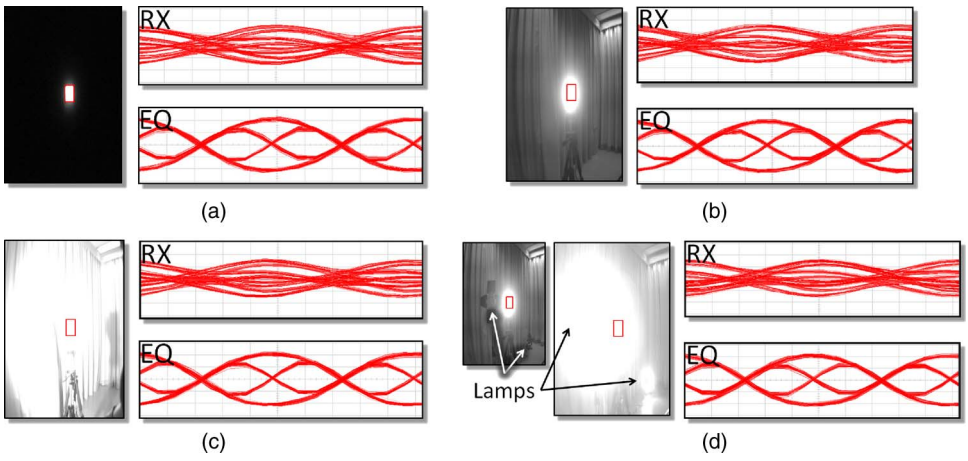

Fig. 21. Experimental results of under various lighting conditions. (a) 0.04 lx. (b) 350 lx. (c) 10,000 lx. (d) Strong lights (backlit condition).

Fig. 19(b) shows the result of a 10 Mbps optical signal reception. As can be seen in this figure, sufficient output amplitude (approximately 50 mV) for signal processing is obtained at 10 MHz signal which is the highest pulse frequency of the 10 Mbps MC. This amplitude value is the result of 9-ch output summing. More specifically, the output per channel is approximately 5.5 mV. In conformity with the frequency response result, the output amplitude is significantly altered by the frequency value difference.

Fig. 20 shows eye diagrams of the RX and EQ signal. As can be seen in the figure, the RX signal is distorted by anomalous response characteristics of the CPx. Thus, the eye pattern is closed. However, the equalizer accurately corrects the distorted RX and the eye is opened sufficiently to permit error-free communication, as shown in (b).

5.4. Experiments Under Various Lighting Conditions

In this section, experimental results obtained under various lighting conditions are shown. Outdoor lighting environments are simulated at 0.04, 350, and 10,000 lx, as well as backlit conditions. These illuminance values are obtained using a background light source radiating towards the LED transmitter. The experimental setting is identical with the previous experiments except for lighting conditions.

Fig. 21 shows gray images, the RX and EQ eye diagrams of each lighting condition. From these results, it can be seen that the EQ remains undisturbed even if the lighting environment is changed. Fig. 21(d) is especially noteworthy as it shows that the IS-OWC "noninterference" characteristic performs as expected.

5.5. Experiments Changing Communication Distance

In this subsection, the experimental results obtained by changing the communication distance are shown. The experimental settings are the same as those used in the previous subsection except for distance changes at 0.5, 1.0, and 2.0 m. As shown in Fig. 22, the EQ remains very stable even if the

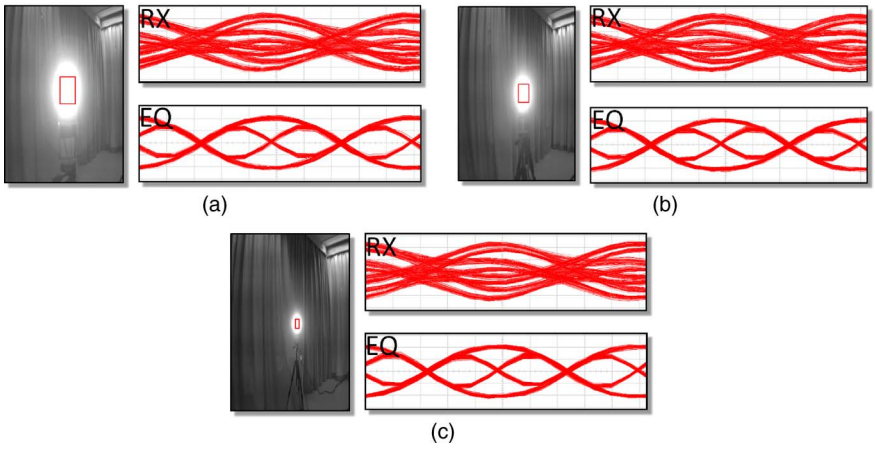

Fig. 22. Experimental results of communication distance changes. (a) 0.5 m. (b) 1.0 m. (c) 2.0 m.

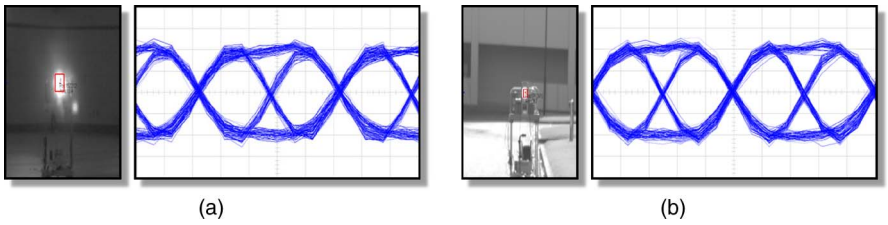

Fig. 23. Experimental results of long communication distances. (a) At 10 m and indoor. (b) At 20 m and outdoor.

communication distance changed. In conformity with the previous experiment, these results show that one of primary IS-OWC characteristics, "stable reception signal power", works as envisioned at these settings.

Fig. 23 shows long distance and 10 Mbps transmission results using an $f = 50$ mm lens. Fig. 23(a) is the EQ signal at approximately 10 m and indoor conditions, and Fig. 23(b) is the EQ signal at approximately 20 m and outdoor conditions. These results show that the high-speed and long distance transmission is permitted by only changing the lens as previous explained. Note, in this long distance experiment only, a few component parts of the receiver system are different, such as the ADC for the communication signal sampling.

5.6. Experiments Releasing All Functions of IS-OWC System, and BER Measurements

This subsection shows the transmission results at 10, 15, and 20 Mbps with BER measurements. While the experimental conditions are similar to those used in the previous subsection, camera receiver movement is introduced to simulate actual usage conditions, as shown in Fig. 24(a). In these experiments, the camera receiver is turned at approximately 1 rotation/s, so the optical signal is received while the LED transmitter in the image is tracked. During the fixed camera condition experiment, the LED detection function is stopped. During the moving camera condition experiment, all the LED detection circuits are activated. In the BER measurement, 10^7 bits are sent without error correction.

Fig. 24(b) shows EQ eye diagrams of the fixed state at each data rate. From these results, it can be seen that an eye pattern is clearly open at 10 and 15 Mbps. Additionally, at 20 Mbps, a relatively good eye result is achieved. During the moving state experiments, the received signal is found to be contaminated by noises at all data rates, as shown in Fig. 24(c). Activating peripheral circuits for the LED detection provoke these noises which are mixed with communication signals, such as

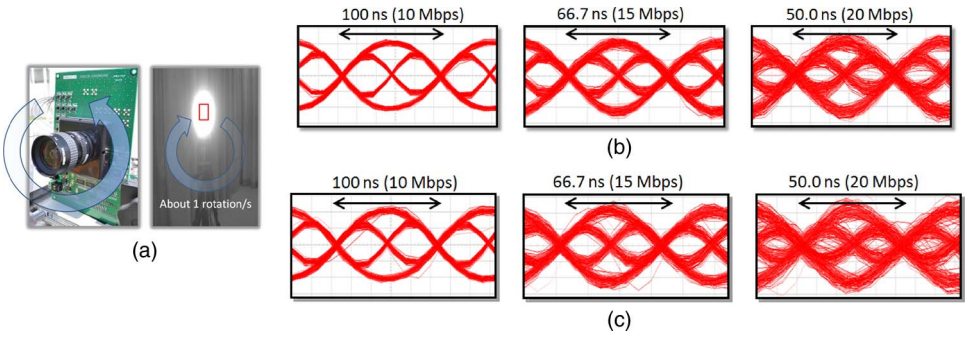

Fig. 24. Changing data rate experiments under fixed and moving conditions. (a) Condition of moving the camera. (b) Fixed conditions. (c) Moving conditions.

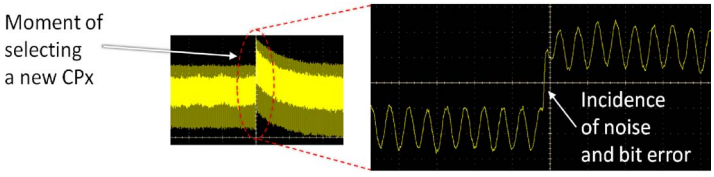

Fig. 25. Received signal when a new position CPx is selected.

TABLE 3

Measurement results of the BER

Data rate	Fixed condition		Moving condition	
10 Mbps	-	(0 / 1×10^7 bit)	-	(0 / 1×10^7 bit)
15 Mbps	-	(0 / 1×10^7 bit)	6.67×10^{-5}	(667 / 1×10^7 bit)
20 Mbps	6.73×10^{-5}	(673 / 1×10^7 bit)	1.25×10^{-3}	(12465 / 1×10^7 bit)

propagations of signals for H. and V. shift register drives. As one example, there is a major noise generated in a 16.6 ms period corresponding to the LED detection timing, as shown in Fig. 25. More specifically, this appears when the X- and Y- address generators select the next CPx at the same time. This result is because the next-selected CPx output line has a different offset voltage condition and is connected to the readout circuit line. In fact, this is transient response that is caused by connecting lines that has discontinuous offset voltage conditions. This noise has the potential to cause 1 or 2 bit errors, depending on the data rate. The noise effect is minor at 10 Mbps, however, degradation of the eye pattern is especially notable at 20 Mbps.

Table 3 shows the BER measurement results. The results of both 10 Mbps conditions and the 15 Mbps fixed condition are error-free. In the 20 Mbps fixed condition and the 15 Mbps moving condition results, the 10^{-5} order is achieved. This is considered to be good performance for wireless communication systems. Furthermore, at 20 Mbps, the BER 10^{-3} is obtained. Using common error correction techniques such as the Reed-Solomon coding and the BCH coding, it is expected that error-free or 10^{-5} BER performance could be easily achieved. Furthermore, should the noise problem be solved, it is expected that BER performance will show significant improvements, even without error correction. There are possible countermeasures for most of these noises, such as the insertion of shield layers between signal lines and accord of offset voltage conditions of each CPx output line. Such countermeasures are not particularly difficult and can be expected to be incorporated into the OCI in the near future.

From these results, it can be concluded that, in the case of real-time LED detection activation, our current system is capable of communications at 15 Mbps per pixel without resorting to error correction, and potentially, our system will provide 20 Mbps per pixel transmission.

6. Conclusion

This paper has presented a novel OWC system consisting of an LED transmitter and camera receiver that is targeted at automotive applications, and introduced its characteristics and capabilities. To achieve the 10 Mbps class data rate and the real-time LED detection, a novel CMOS image sensor called an OCI has been developed and installed in the camera receiver. Two key technologies are especially important during development of the OCI: the CPx for high-speed signal reception and the 1-bit flag image output function for quick and accurate LED detection. These technologies are successfully incorporated into the OCI.

Using this developed OCI, our first IS-OWC system has been completed. A new LED detection method using the 1-bit flag image have been proposed, and experiments have been conducted during which the detection performance and availability of the method are confirmed in 16.6 ms real-time operating conditions. This technology is expected to be extremely helpful when this system is used in actual road (outdoor) environments.

Furthermore, owing to our specialized pixel, the CPx, a 15 Mbps data rate per pixel is achieved and the potential of the 20 Mbps transmission is also shown while simultaneously conducting LED detection in real-time. Additionally, robust communication performance to changing distances and lighting conditions is also confirmed. However, we also determine that our current system suffers from noise contamination imposed by peripheral circuit operations. Hereafter, eliminating this noise via circuit remediation designing is seen as a key issue related to reception performance improvements.

Based on these developments and the experimental results discussed above, we believe this system has strong potential for used in automotive applications. In the future, we expect to adapt the system for use in actual automotive communication systems and intend to conduct field trials of this system under more arduous movement and lighting conditions.

Additionally, while this paper focuses on the automotive applications, it is believed that the system can be useful in other areas, such as factory automation, mobile phones, and wireless LAN networks, and that such new field uses should be considered seriously. Furthermore, it is also believed that the IS-OWC system's ability to fuse communication and image processing results has potential for prompting emergence of unprecedented new applications.

References

[1] M. Nakagawa, "Visible light communications," in *Proc. Conf. Lasers Electro-Opt.*, May 2007, pp. 1–2.

[2] R. Mesleh, H. Elgala, and T. D. C. Little, "A novel method to mitigate LED nonlinearity distortions in optical wireless OFDM systems," in *Proc. OFC/NFOFC*, Mar. 2013, pp. 1–3.

[3] D. Tsonev, S. Sinanovic, and H. Hass, "Novel unipolar orthogonal frequency division multiplexing (U-OFDM) for optical wireless," in *Proc. IEEE 75th Veh. Technol. Conf.*, May 2012, pp. 1–5.

[4] L. Zeng, D. O'Brien, H. Minh, G. Faulkner, K. Lee, D. Jung, Y. Oh, and E. T. Won, "High data rate multiple input multiple output (MIMO) optical wireless communications using white LED lighting," *IEEE J. Sel. Areas Commun.*, vol. 27, no. 9, pp. 1654–1662, Dec. 2009.

[5] *Visible Light Communication Consortium*. [Online]. Available: http://www.vlcc.net/?ml_lang=en

[6] M. Z. Afgani, H. Hass, H. Elgala, and D. Knipp, "Visible light communication using OFDM," in *Proc. 2nd Int. Conf. TRIDENTCOM*, 2006, p. 134.

[7] C. W. Chow, C. H. Yeh, Y. Liu, and Y. F. Liu, "Digital signal processing for light emitting diode based visible light communication," *IEEE Photon. Soc. News*, vol. 26, no. 5, pp. 9–13, Oct. 2012.

[8] A. M. Vegni and T. D. C. Little, "Handover in VLC systems with cooperating mobile devices," in *Proc. Int. Conf. Comput., Netw. Commun.*, Jan. 2012, pp. 126–130.

[9] T. Komine and M. Nakagawa, "Fundamental analysis for visible-light communication system using LED lightings," *IEEE Trans. Consum. Electron.*, vol. 50, no. 1, pp. 100–107, Feb. 2004.

[10] D. O'brien, L. Zeng, H. Le-Minh, G. Faulkner, J. W. Walewski, and S. Randel, "Visible light communications: Challenges and possibilities," in *Proc. IEEE PIMRC*, 2008, pp. 1–5.

[11] S. Kitano, S. Haruyama, and M. Nakagawa, "LED road illumination communications system," in *Proc. IEEE 58th Veh. Technol. Conf.*, 2003, pp. 3346–3350.

[12] S. Okada, T. Yendo, T. Yamazato, T. Fujii, M. Tanimoto, and Y. Kimura, "On-vehicle receiver for distant visible light road-to-vehicle communication," in *Proc. IEEE Intell. Veh. Symp.*, Jun. 2009, pp. 1033–1038.

[13] M. Akanegawa, Y. Tanaka, and M. Nakagawa, "Basic study on traffic information system using LED traffic lights," *IEEE Trans. Intell. Transp. Syst.*, vol. 2, no. 4, pp. 197–203, Dec. 2001.

[14] A. Cailean, B. Cagneau, L. Chassagne, S. Topsu, Y. Alayli, and J.-M. Blosseville, "Visible light communications: Application to cooperation between vehicle and road infrastructures," in *Proc. Intell. Veh. Symp. (IV)*, Jun. 2012, pp. 1055–1059.
[15] S. Haruyama, "Visible light communication," in *Proc. Int. Display Workshop*, 2010, pp. 2189–2192.
[16] H. B. C. Wook, T. Komine, S. Haruyama, and M. Nakagawa, "Visible light communication with LED-based traffic lights using 2-dimensional image sensor," in *Proc. IEEE CCNC*, 2006, vol. 1, pp. 243–247.
[17] M. Yoshino, S. Haruyama, and M. Nakagawa, "High-accuracy positioning system using visible LED lights and image sensor," in *Proc. IEEE Radio Wireless Symp.*, Jan. 2008, pp. 439–442.
[18] H. S. Liu and G. Pang, "Positioning beacon system using digital camera and LEDs," *IEEE Trans. Veh. Technol.*, vol. 52, no. 2, pp. 406–419, Mar. 2003.
[19] N. Iizuka, "Image sensor communication—A new way of visible light communication," in *Proc. Int. Display Workshop*, 2010, pp. 2193–2196.
[20] Y. Oike, M. Ikeda, and K. Asada, "A smart image sensor with high-speed feeble ID-beacon detection for augmented reality system," in *Proc. 29th ESSCIRC*, Sep. 2003, pp. 125–128.
[21] N. Matsushita, D. Hihara, T. Ushiro, S. Yoshimura, J. Rekimoto, and Y. Yamamoto, "ID CAM: A smart camera for scene capturing and ID recognition," in *Proc. IEEE and ACM Int. Sym. Mixed Augmented Reality*, 2003, pp. 227–236.
[22] D. Yamanaka, S. Haruyama, and M. Nakagawa, "The design of high-speed image sensor chip for receiving the data of visible-light ID system," (in Japanese), *IEICE Techn. Rep.*, vol. 107, no. 300, pp. 97–102, Oct. 2007.
[23] S. Nishimoto, T. Nagura, and T. Yamazato, "Overlay coding for road-to-vehicle visible light communication using LED array and high-speed camera," in *Proc. 14th Int. IEEE Conf. Intell. Transp. Syst.*, 2011, pp. 1704–1709.
[24] S. Itoh, I. Takai, M. Z. Sarker, M. Hamai, K. Yasutomi, M. Andoh, and S. Kawahito, "A CMOS image sensor for 10 Mb/s 70 m-range LED-based spatial optical communication," in *Proc. IEEE ISSCC, Dig. Tech. Papers*, San Francisco, CA, USA, Feb. 2010, pp. 402–403.
[25] M. S. Z. Sarker, I. Takai, M. Andoh, K. Yasutomi, S. Itoh, and S. Kawahito, "A CMOS imager and 2-D light pulse receiver array for spatial optical communication," in *Proc. IEEE Asian Solid-State Circuits Conf.*, Nov. 2009, pp. 113–116.
[26] M. S. Z. Sarker, S. Itoh, M. Hamai, I. Takai, M. Andoh, K. Yasutomi, and S. Kawahito, "Design and implementation of a CMOS light pulse receiver cell array for spatial optical communications," *Sensors*, vol. 11, no. 2, pp. 2056–2076, Feb. 2011.
[27] N. Teranishi, A. Kohono, Y. Ishihara, E. Oda, and K. Arai, "No image lag photodiode structure in interline CCD image sensor," in *Proc. Int. Electron Dev. Meet.*, 1982, vol. 28, pp. 324–327.
[28] P. P. K. Lee, R. C. Gee, R. M. Guidash, T.-H. Lee, and E. R. Fossum, "An active pixel sensor fabricated using CMOS/CCD process technology," in *Proc. Workshop CCD AIS*, 1995, pp. 115–119.
[29] J. Nakamura, *Image Sensor and Signal Processing for Digital Still Cameras*. Boca Raton, FL, USA: CRC Press, 2006.
[30] M. B. Dillencourt, "A general approach to connected-component labeling for arbitrary image representations," *J. ACM*, vol. 39, no. 2, pp. 253–280, Apr. 1992.